BaWO$_4$:Ce Single Crystals Codoped with Na Ions

Slawomir M. Kaczmarek [1,*], Grzegorz Leniec [1] , Tomasz Bodziony [1], Hubert Fuks [1],
Zbigniew Kowalski [1], Winicjusz Drozdowski [2] , Marek Berkowski [3], Michal Głowacki [3] ,
Marcin E. Witkowski [2] and Michal Makowski [2]

[1] Institute of Physics, Faculty of Mechanical Engineering and Mechatronics,
West Pomeranian University of Technology in Szczecin, Al. Piastów, 17, 70-310 Szczecin, Poland;
taran@zut.edu.pl (G.L.); tbodziony@zut.edu.pl (T.B.); fux@zut.edu.pl (H.F.); zwkowalski@gmail.com(Z.K.)

[2] Institute of Physics, Faculty of Physics, Astronomy and Informatics, Nicolaus Copernicus University,
Grudziadzka 5, 87-100 Torun, Poland; wind@fizyka.umk.pl (W.D.); mwit@fizyka.umk.pl (M.E.W.);
mimak@fizyka.umk.pl (M.M.)

[3] Institute of Physics, Polish Academy of Sciences, Aleja Lotnikow 32/46, PL-02668 Warsaw, Poland;
berko@ifpan.edu.pl (M.B.); glowacki@ifpan.edu.pl (M.G.)

* Correspondence: skaczmarek@zut.edu.pl or smkaczmar@wp.pl; Tel.: +48-91-449-4887

Abstract: Single crystals of BaWO$_4$, BaWO$_4$: 0.5 at. % Ce; BaWO$_4$: 1 at. % Ce; BaWO$_4$: 0.5 at. % Ce, 1 at. % Na; and BaWO$_4$: 1 at. % Ce, 2 at. % Na were grown from an inductively heated iridium crucible by the Czochralski method on a Malvern MSR4 puller. They were investigated using Electron Paramagnetic Resonance (EPR) spectroscopy at helium temperatures. One isolated center of high (D$_{2d}$ or S$_4$) symmetry was found and two or more other centers of lower symmetry were identified, depending on crystal doping. From the fitting using the EPR-NMR program, the following parameters of g-matrix for the high symmetry center were found: g$_x$ = 1.505, g$_y$ = 1.505, and g$_z$ = 2.731. The linewidth vs. temperature revealed an increasing exponential tendency with increasing temperature. It showed one phonon at the lower temperatures and a Raman + Orbach effect at the higher temperatures. Radioluminescence and pulse height spectra showed rather poor scintillation properties, without any contribution from cerium emission.

Keywords: scheelite; BaWO$_4$; structural refinement; EPR; roadmap; local symmetry

1. Introduction

Barium tungstate (BaWO$_4$) crystals are an interesting and relatively new medium for stimulated Raman scattering for applications in Raman shifters of laser radiation [1]. BaWO$_4$ has the largest energy gap among several tungstates with a scheelite structure, space group $I4_1/a$, equal to 5.26 eV [2]. Barium tungstate is a widely investigated inorganic optical material due to its attractive emission properties. The properties strongly depend on the crystal structure and morphology. The same dependence shows the photocatalytic properties of the crystal [3].

The Ce^{3+}-doped and undoped samples of alkali earth metal tungstates MWO$_4$ (M=Ca, Sr, and Ba) microcrystalline phosphors were synthesized by a co-precipitation method in a controlled pH environment by Double et al. [3]. X-Ray Diffraction (XRD) pattern and Scanning Electron Microscopy (SEM) micrographs revealed the formation of the desired tetragonal phase of the scheelite-type structure with the grain size of a few micrometers. Phosphor excited by 280 nm showed a broad emission band in the visible region (400–650 nm), with a peak in the blue region at around 465 nm, which is characteristic of the (WO$_4$)$^{2-}$ complex. More extended investigations and quantum mechanical calculations from the morphology point of view were performed for BaWO$_4$ crystals obtained using the same technique by Oliveira et al. [4]. Liu et al. explored the growth mechanism leading to the

observed range of morphologies through in situ Transmission Electron Microscopy (TEM) and in situ Atomic Force Microscopy (AFM) [5]. Ke et al. have provided an integrated overview of the fundamentals and recent progress of MWO_4-based photocatalysts [6]. Oliveira et al. also investigated the photoluminescence spectrum in $BaWO_4$ crystals centered at about 522 nm. They assigned the emission to the charge transfer in the $[MO_4]^{2-}$ (M = Mo and W) complex [7]. Yellow emission was reported from $BaWO_4$: Sm^{3+} phosphors by Shi et al. [8].

Good quality $BaWO_4$ crystals can be grown by the Czochralski technique and doped with rare-earth ions [9–11]. We have grown pure $BaWO_4$, as well as $BaWO_4$ doped with 0.5 at. % Ce and 1 at. % Ce, single crystals using the above technique. The absorption and emission spectra of the crystals were investigated by Włodarczyk et al. in [12]. In the UV, the crystals showed typical absorption for Ce^{3+}, with two bands that peaked at 320 nm and 285 nm, being associated with lowest energy 4f-5d transitions. However, only very weak Ce^{3+} luminescence was observed, even at 10 K, contrary to the above-mentioned report on this subject [3].

Doping with trivalent ions requires charge compensation which may be provided, for example, by structural defects or proper co-doping with alkaline metal ions. Voronina et al. obtained $BaWO_4$: Nd^{3+} single crystals by the Czochralski method using compensating dopants: Nb^{5+} and Na^+ [13]. Therefore, we decided to co-dope the crystals with Na ions. In this paper, we analyze local symmetries of cerium ions in $BaWO_4$:0.5 at. % Ce; $BaWO_4$:1 at. % Ce; $BaWO_4$:0.5 at. % Ce, 1 at. % Na; and $BaWO_4$:1 at. % Ce, 2 at. % Na single crystals. Radioluminescence spectra and light yield measurements of the above crystals and pure $BaWO_4$ are also presented and discussed for comparison.

2. Materials and Methods

Single crystals of $BaWO_4$; $BaWO_4$:0.5 at. % Ce; $BaWO_4$:1 at. % Ce; $BaWO_4$: 0.5 at. % Ce, 1 at. % Na; and $BaWO_4$:1 at. % Ce, 2 at. % Na were grown from an inductively heated iridium crucible by the Czochralski method on a Malvern MSR4 puller. The reagents—$BaCO_3$ (5N), WO_3 (4N), CeO_2 (4N), and Na_2CO_3(5N) (Sigma – Aldrich, Poznań, Poland r Fluka, Poznań, Poland)—were dried in 300 °C for 12 h before weighing and mixing them in stoichiometric molar ratios. Starting materials were pressed into cylindrical pellets and then put into the crucible, which was 40 mm in diameter. $BaWO_4$ single crystals were grown on an iridium rod used as a seed with a pulling rate of 3 mm/h and a speed of rotation of 20 rpm in ambient (N_2) atmosphere. Obtained crystal boules of a 20 mm diameter and 40 mm length were colorless and transparent (Figure 1). $BaWO_4$: Ce crystals co-doped with Na show some cracks.

Phase analysis and structural refinement were performed on powdered single crystals by X-ray powder diffraction using Ni-filtered Cu-K_α radiation with a Siemens D5000 diffractometer (Siemens, München, Germany). Data were collected in the range $10° < 2\Theta < 110°$, with a step o 0.02° and an averaging time of 10 s/step. The powder diffraction patterns were analyzed by the Rietveld refinement method using the DBWS-9807 program.
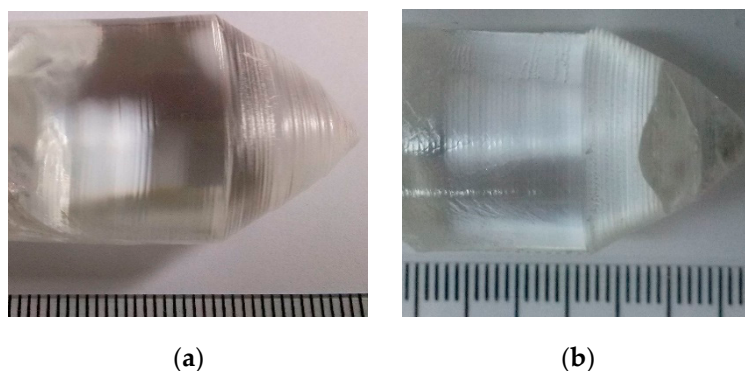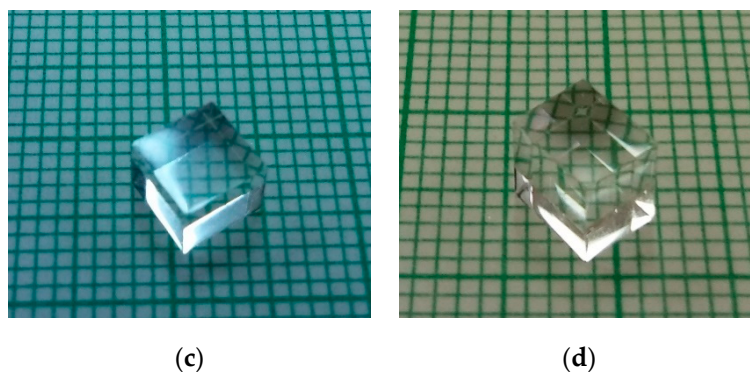

(**a**)   (**b**)

Figure 1. *Cont*.

(c)   **(d)**

Figure 1. $BaWO_4$: Ce single crystals (mm) and cubes ($5 \times 5 \times 5$ mm): (**a,c**). 0.5 at. %, (**b,d**). 1 at. % obtained by the Czochralski method.

The structure of the $BaWO_4$ single crystal is shown in Figure 2. From the local symmetry point of view, among three planes distinctly different seems to be an ab-plane. The space group is $I4_{1/a}$ and symmetry C^6_{4h}, in which Ba atoms are coordinated to eight O atoms, while W atoms exhibit a tetragonal coordination of O atoms; thus, the building blocks of the $BaWO_4$ crystal are deltahedral $[BaO_8]$ and tetrahedral $[WO_4]$ clusters [14].
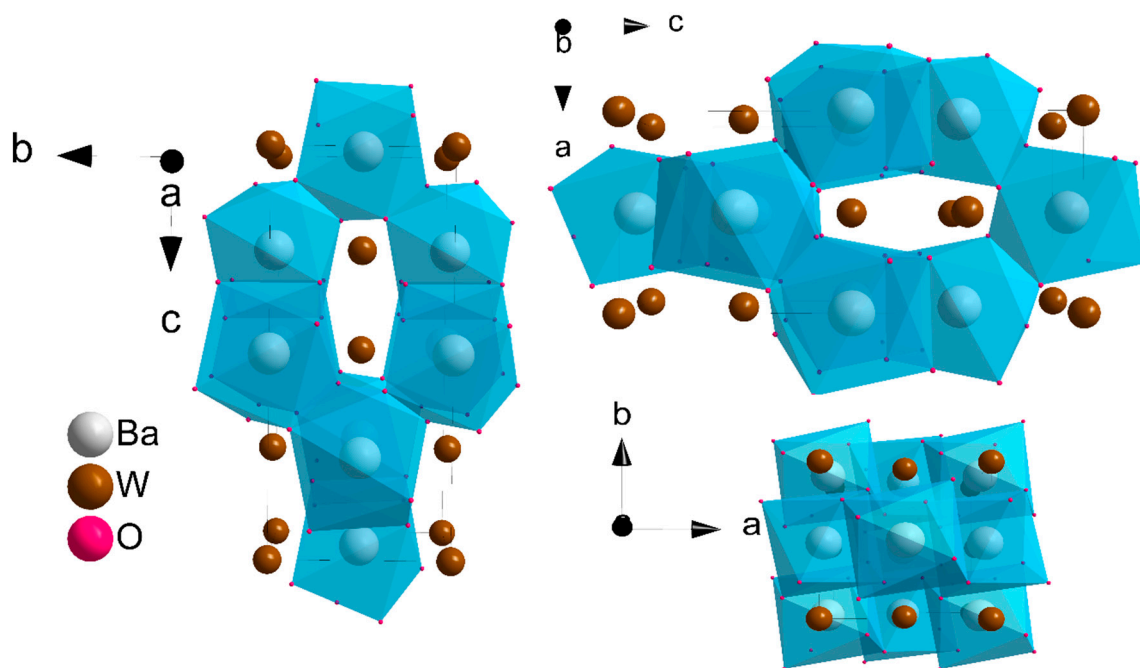

Figure 2. The structure of $BaWO_4$ in three directions [14].

The EPR spectroscopic measurements were carried out using a standard X-band Bruker E-500 EPR spectrometer (Karlsruhe, Germany) with the magnetic induction range 0–1.4 T, the micro field modulation of 100 kHz, and the temperature range (3–300) K.

The magnetic induction was scaled with an NMR magnetometer. Measurements were performed under the flow of helium gas, using an Oxford Instruments (Abingdon, Oxfordshire, England) flowing liquid He cryostat to control the temperature. The samples used for EPR purposes have been shaped as $2.5 \times 2.5 \times 3.5$ mm^3 parallelepipeds with planes perpendicular to crystallographic axes. In order to determine the local symmetry and localization of the paramagnetic probe in the crystal lattice, the angular dependences of Ce^{3+} have been drawn (Figures 5, 7 and 8). The laboratory axis system (LAS; *a, b, c*) corresponded to the crystallographic axis system (CAS; *x, y, z*). Axes *a*, *b*, and *c* were perpendicular to the magnetic induction *B*. The EPR-NMR program was used to find spin-Hamiltonian

parameters [15]. The *g*-factors were obtained by the complete diagonalization of the spin Hamiltonian and least-squares fitting to the observed spectra.

Radioluminescence spectra at various temperatures between 10 and 350 K were recorded with a custom-made set-up consisting of an Inel X-ray generator with a Cu-anode tube (Artenay, Loiret, France), an ARC SP-500i monochromator (Acton, MA, USA), a Hamamatsu R928 photomultiplier tube (Hamamatsu City, Shizuoka, Japan), and an APD Cryogenics closed-cycle helium cooler (Allentown, PA, USA) controlled with a Lake Shore 330 unit (Westerville, OH, USA). Pulse height spectra were measured at room temperature (RT) under gamma excitation from a ^{137}Cs source (662 keV). The dedicated set-up consisted of a Hamamatsu R2059 photomultiplier tube (Hamamatsu City, Shizuoka, Japan), a Canberra 2005 integrating preamplifier (Meriden, CT, USA), a Canberra 2022 spectroscopy (Meriden, CT, USA) amplifier (with shaping time adjusted at 12 µs), and a Tukan 8 k USB multichannel analyzer (Świerk, Poland).

3. X-ray Measurements

The X-ray diffraction patterns for all the crystals investigated are presented in Figure 3. The measurements were performed at room temperature. The diffraction peak positions and intensities of all of the investigated crystals are consistent with the Joint Committee on Powder Diffraction Standards (JCPDS) Card No: 43-0646 of $BaWO_4$. The structure of the crystals is tetragonal and belongs to the $I4_1/a$ space group. Lattice parameters have been determined as $a = 5.6149(1)$ Å, $c = 12.7201(2)$ Å for $BaWO_4$: 0.5 at. % Ce; $a = 5.6152(1)$ Å, $c = 12.7209(3)$ Å for $BaWO_4$: 1 at. % Ce; $a = 5.6180(1)$ Å, $c = 12.7141(2)$ Å for $BaWO_4$: 0.5 at. % Ce, 1 at. % Na; and $a = 5.619(1)$ Å, $c = 12.717(2)$ Å for $BaWO_4$: 1 at. % Ce, 2 at. % Na. The pure $BaWO_4$ has a tetragonal structure with unit cell dimensions of a = 5.61 Å, c = 12.71 Å [16]. Rocking curves for the symmetrical (400) reflections have shown the following values of FWHM: 0.047°, 0.052°, 0.108°, and 0.126° for $BaWO_4$: 0.5 at. % Ce; $BaWO_4$: 1 at. % Ce; $BaWO_4$: 0.5 at. % Ce, 1 at % Na; and $BaWO_4$: 1 at. %Ce, 2 at % Na, respectively. This indicates a good enough quality of the crystals.
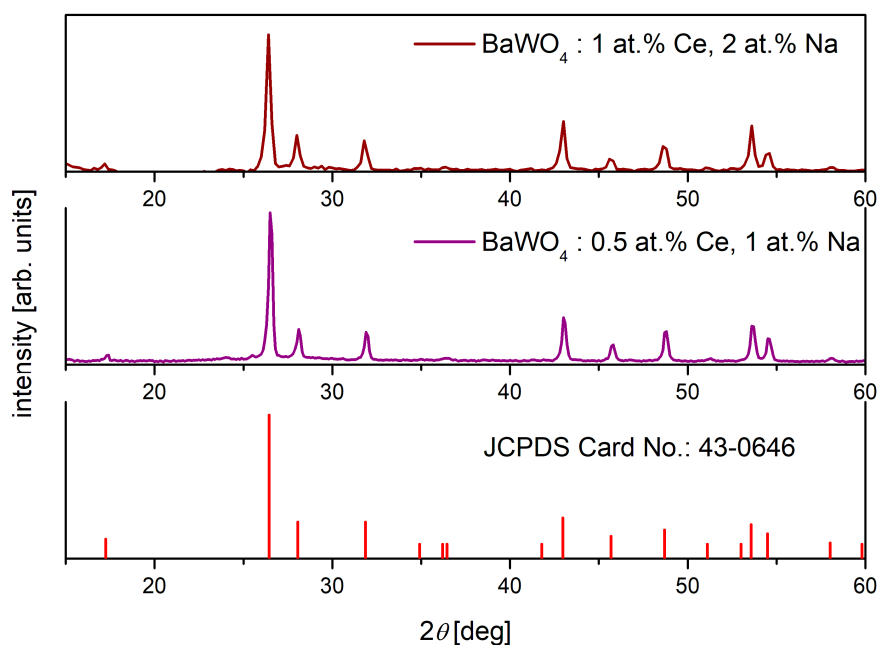

Figure 3. Diffractograms of the analyzed $BaWO_4$ single crystals doped with cerium and co-doped with sodium ions. The red diffractogram indicates the position and relative intensity of JCPDS card no.: 43-0646.

Ce^{3+} ions are only expected to substitute for Ba^{2+} ions in the $BaWO_4$ structure owing to the respective ionic radii of cations ($Ce^{3+} - R = 1.143$ Å, $Ba^{2+} - R = 1.142$ Å, $W^{6+} - R = 0.74$ Å, $Na^+ - R = 1.18$ Å). In the $BaWO_4$ crystal, barium ions have four different crystallographic positions.

4. EPR Results

Due to the complexity of the obtained EPR results (many high and low symmetry centers), we only concentrate on the influence of sodium co-doping on crystal quality. The results of EPR studies of $BaWO_4$: Ce crystals and crystals co-doped with Na for several temperatures are presented in Figure 4.
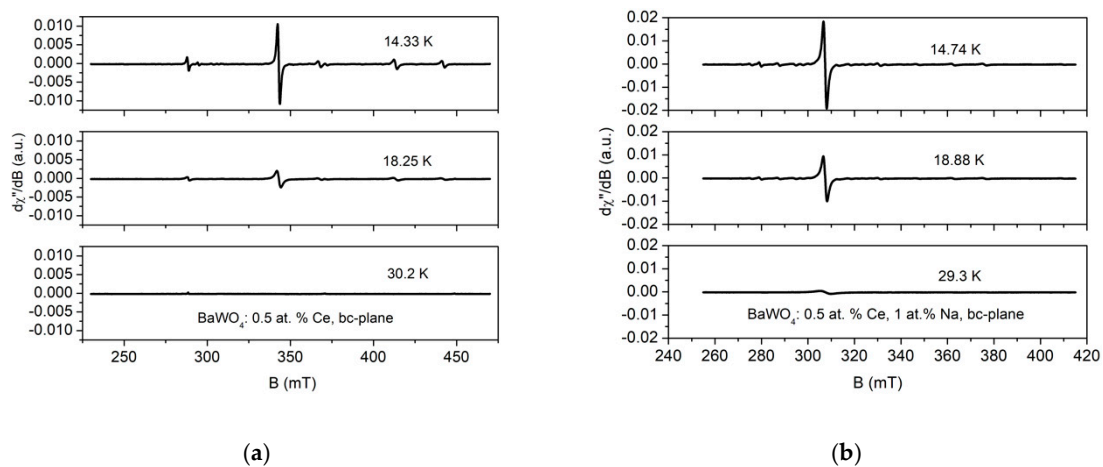

(a)   (b)

Figure 4. EPR spectra of $BaWO_4$:0.5 at. Ce (**a**) and $BaWO_4$:0.5 at. % Ce, 1 at. % Na (**b**) for several temperatures.

The EPR signal consists of one intense (main) EPR line and four or more weaker EPR lines assigned to cerium ions at different symmetry sites. The latter appear due to the substituting of some cerium ions at interstitial positions in view of different valences between barium (2+) and cerium (3+) ions (vacant compensation) and the presence of sodium co-dopant (vacant and co-dopant compensation). They all vanish over 60 K, as is usual for rare-earth ions. As cerium has no isotope with non-zero nuclear spin, the EPR spectrum of Ce^{3+} in a single crystallographic site is usually composed of a single line. The free cerium (Ce^{3+}) ion has a $4f^1$ electronic configuration. A low symmetry of Ce^{3+} sites in the investigated crystals splits the six-fold degenerated $^2F_{5/2}$ ground state into three degenerate levels, referred to as Kramers doublets. Only the lowest doublet is populated at liquid helium temperature, so the cerium ions system can be described by a fictitious spin $S = 1/2$. Thus, cerium is a Kramers ion with $S = 1/2$, $L = 3$, and $J = 5/2$, where S, L, and J are the spin, orbital, and total momentum, respectively.

The crystals co-doped with sodium seem to have a higher real concentration of cerium ions than those which are single doped. The same conclusions can be derived for the other two investigated crystals. Therefore, we assigned the following spin-Hamiltonian to analyze the local symmetry of cerium ions:

$$H_s = \mu_B B g S \tag{1}$$

In Figure 5, the roadmap of the main center in all planes: *ab*, *bc*, and *ca* for $BaWO_4$: 0.5 at. % Ce crystal is presented. From the fitting of Equation (1) using the EPR-NMR program, the following parameters of *g*-matrix for the center can be assigned to $g_x = 1.506(1)$, $g_y = 1.506(1)$, and $g_z = 2.712(2)$ (see Table 1).

Temperature dependence of the EPR line has shown ferromagnetic-like interactions between cerium ions, with Curie-Weiss temperature, $\Theta \sim 1$ K. The linewidth vs. temperature revealed an increasing exponential tendency with increasing temperature. It shows one phonon at the lower temperatures and a Raman + Orbach effect (Figure 6) at the higher temperatures, according to the equation $B = B_o + A\exp(-W/kT)$, where $B_o = 1.12$ mT, $A = 1390$ mT, and $W/k = 173$ K. Exponential

change of the B could be connected with the spin-lattice relaxation processes involving excited states of Ce^{3+} ions.
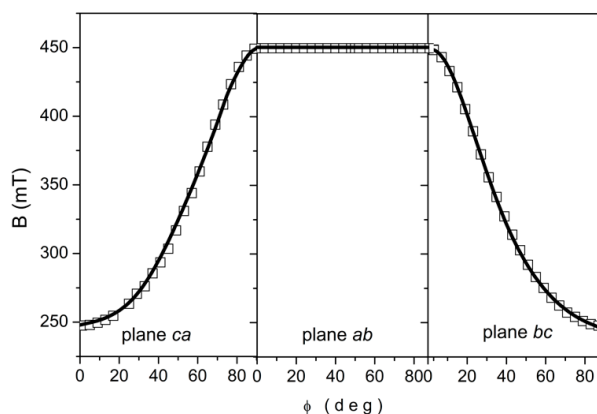

Figure 5. The angular dependencies of resonance line positions of the main center measured when crystal (BaWO$_4$: Ce^{3+} 0.5%) is rotating perpendicularly to *a*, *b*, and *c* laboratory axis at a temperature of ~8 K.

Table 1. Hamiltonian parameters of Ce^{3+} ions in the BaWO$_4$ crystal.

| BaWO$_4$	g_x	g_y	g_z	Tilt (deg)	Symmetry
	1.506(1)	1.506(1)	2.712(2)	-	C$_4$
Ce^{3+} 0.5 at. %	1.40(2)	1.32(1)	2.45(1)	10.0(5)	C$_2$
	1.53(1)	1.64(2)	2.52(1)	11.0(5)	C$_2$
	1.506(1)	1.506(1)	2.712(2)	-	C$_4$
Ce^{3+} 1 at. %	1.38(2)	1.35(1)	2.39(1)	10.0(5)	C$_2$
	1.52(1)	1.64(1)	2.51(1)	11.1(5)	C$_2$
	1.506(1)	1.506(1)	2.712(2)	-	C$_4$
Ce^{3+} 0.5 at. %	1.30(2)	1.48(1)	2.49(1)	10.0(5)	C$_2$
Na$^+$ 1 at. %	1.44(1)	1.46(1)	2.65(1)	4.9(5)	C$_2$
	1.48(1)	1.49(1)	2.68(1)	~0	C$_{2v}$
	1.506(1)	1.506(1)	2.712(2)	-	C$_4$
Ce^{3+} 1 at. %	1.30(2)	1.46(1)	2.63(1)	13.3(2)	C$_2$
Na$^+$ 2 at. %	1.43(2)	1.50(1)	2.68(1)	14.4(2)	C$_2$
	1.48(1)	1.44(1)	2.69(1)	~0	C$_{2v}$
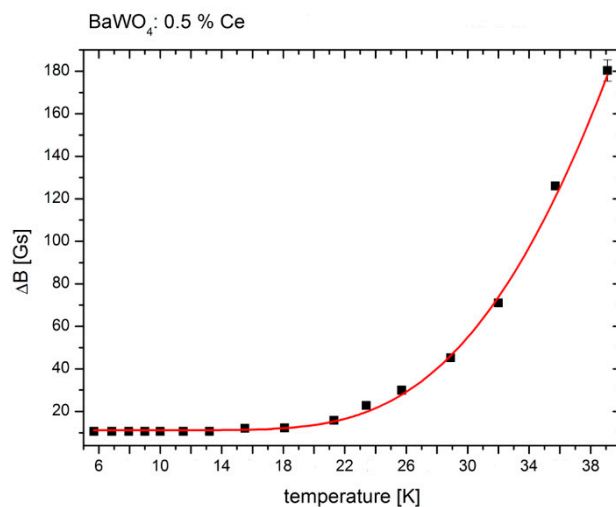
Figure 6. The line shape of the main EPR line vs. temperature (BaWO$_4$:0.5 at. % Ce). The solid line reflects B = B$_o$ + Aexp(−W/kT) dependence.

Besides the central line in the EPR spectrum, corresponding to high symmetry cerium ions (C_4), other lines of lower symmetry are observed in the spectrum. They are seen in Figure 7, where angular dependencies along the three directions *a*, *b*, and *c* for BaWO$_4$: 0.5 at. % Ce single crystal are presented.
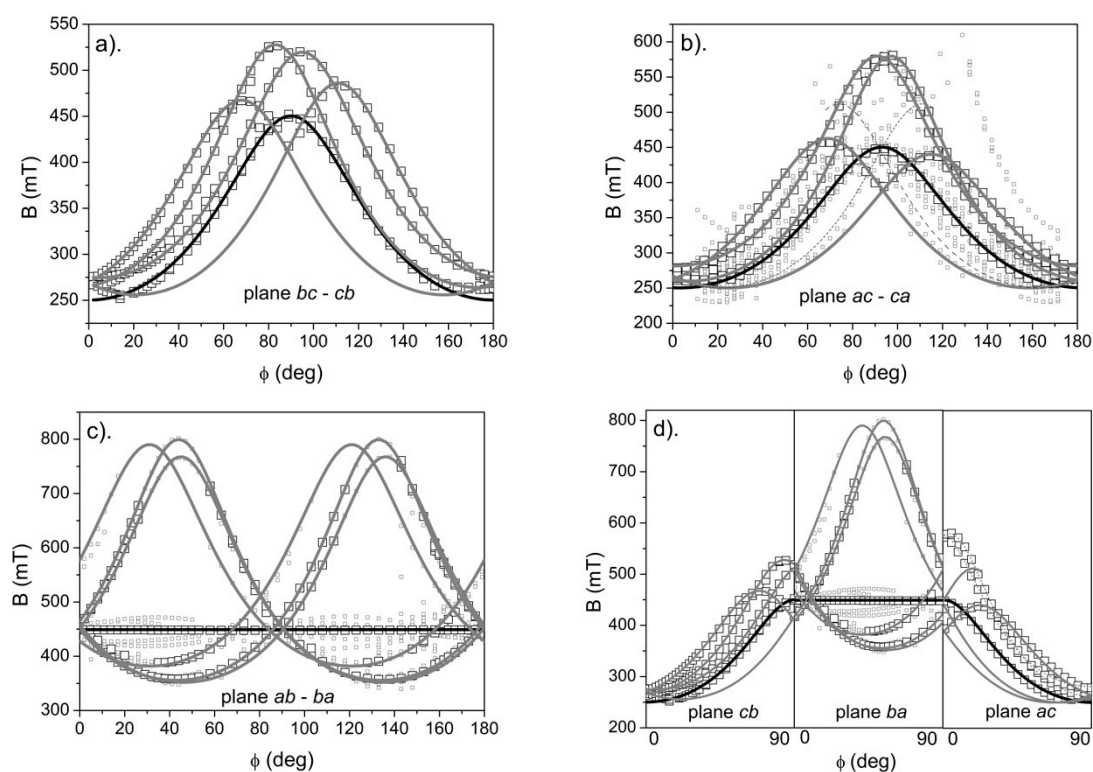

Figure 7. (**a**–**c**). Angular dependencies (roadmaps) along three directions *a*, *b*, and *c* of the BaWO$_4$: 0.5 at. % Ce single crystal. (**d**). Overall angular dependencies.

Axes *a*, *b*, and *c* are perpendicular to the magnetic field induction, **B**. The squares are experimental points and the solid lines are the fitting of the spin Hamiltonian parameters to the paramagnetic center. From Figure 7a–c, one can find that, besides one line of high symmetry (solid line No. 1), there are at least two low symmetry centers. To each of the centers, two lines are assigned due to low symmetry. The symmetry of the centers seems to be C_2. Such a specific structure of the EPR signal, composed of two sets of doublets, indicates the existence of two magnetically inequivalent positions of Ce^{3+} ions for each site. As one can see from Figure 7d, EPR lines do not maintain continuity during a transition from the *c* axis to the *b* axis. This means that the laboratory *c* axis does not correspond to the crystallographic *z* axis. For monoclinic symmetry, this is obvious ($\gamma \neq 90$ deg). The tilt of axis *c* is as high as 10 and 11 degrees for lines 3 (3a and 3b, Figure 7a) and 2 (2a and 2b, Figure 7a), respectively. This confirms the C_2 symmetry of the cerium ions. The same conclusion can be derived from the EPR spectra measured for the BaWO$_4$ single crystal doping with 1% cerium ions. An entire other conclusion can be derived from the spectra of the BaWO$_4$: Ce crystals co-doped with sodium ions.

In Table 1, spin-Hamiltonian parameters, tilt, and the kind of symmetry of the cerium centers are gathered.

In Figure 8, angular dependencies are compared for BaWO$_4$: 0.5 at. % Ce and BaWO$_4$: 1 at. % Ce, 2 at. % Na single crystals, respectively. In the BaWO$_4$: Ce crystals doped with sodium ions, one can distinguish a single line assigned to cerium ions at local symmetry C_4, two doublets assigned to cerium ions at local symmetry C_2, and one doublet responsible for cerium ions at local C_{2v} symmetry. As one can see, EPR lines assigned to low symmetry centers are more symmetric in the case of Na co-doping. This represents a clearer structure of the Na co-doped crystal. It explains the higher real concentration of cerium ions in BaWO$_4$:Ce single crystals co-doped with Na. So, co-doping with Na leads to the

more perfect crystal structure of $BaWO_4$:Ce single crystals and allows a higher real concentration of cerium ions to be introduced. However, it still does not allow photoluminescence (PL) originating from Ce^{3+} ions to be obtained. Spin-Hamiltonian parameters, tilt, and the kind of cerium ions local symmetry for all of the investigated crystals are gathered in Table 1. A more detailed analysis of the EPR properties of $BaWO_4$ single crystals doped with cerium ions is presented in [17].
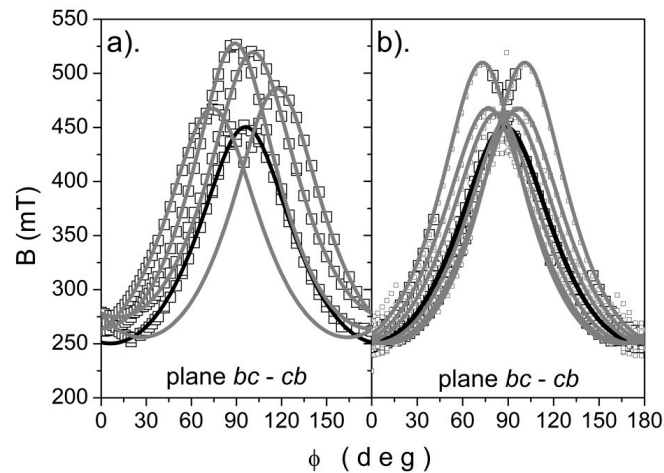

Figure 8. Comparison of angular dependencies for $BaWO_4$: 0.5 at. % Ce (**a**) and $BaWO_4$: 1 at. % Ce, 2 at. % Na (**b**) single crystals.

5. Radioluminescence Measurements

In Figure 9, radioluminescence spectra at selected temperatures from the range (10–350) K are presented for the more representative cases: pure $BaWO_4$ and $BaWO_4$: 0.5 at. % Ce.
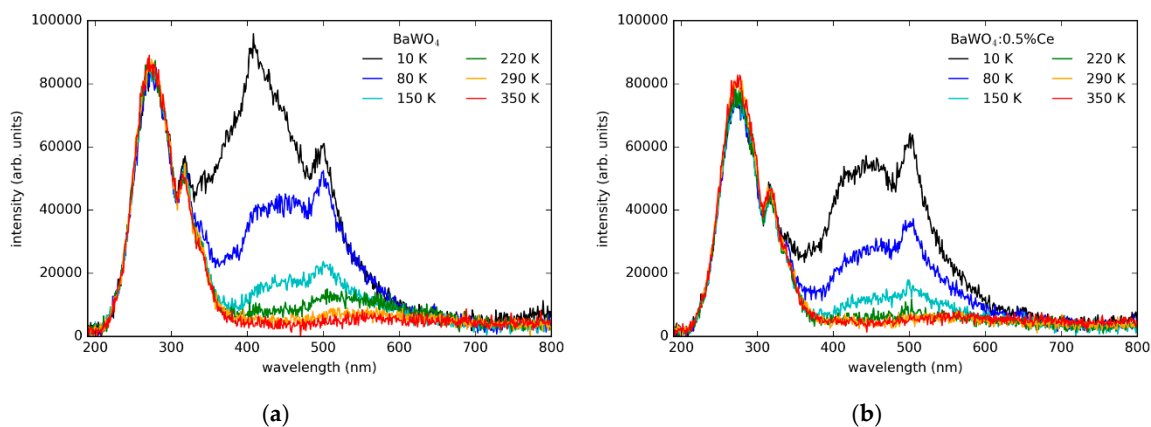

(**a**)   (**b**)

Figure 9. Radioluminescence spectra of $BaWO_4$ (**a**) and $BaWO_4$: 0.5 at. % Ce (**b**) single crystals.

In both cases, two spectral regions can be distinguished. A double band peaking at about 280 and 310 nm is thermally very stable, maintaining the same intensity between 10 and 350 K (against any impression, the spectra have not been normalized). On the contrary, the other band, also with a double structure (peaks at about 410–430 and 500 nm), is strongly quenched with increasing temperature, almost vanishing above RT. Although there are some minor differences, mainly in the case of a longer wavelength band, we suppose that all the emissions are related to the $BaWO_4$ host. Since there are no premises of the Ce^{3+} 5d-4f emission, it seems that either the energy transfer from the $BaWO_4$ host is extremely weak or the 5d levels of Ce^{3+} emerge in the conduction band. We note that Cavalcante et al. have investigated the photoluminescence mechanism of $BaWO_4$ micro-powders and have found that the PL emission is caused by the structural defects and/or distortions on the [WO_4] tetrahedron

groups by the exciting radiation [18]. A strong emission band at about 280 nm was not recorded even by Dabre et al. [3], who analyzed the photoluminescence properties of microcrystalline BaWO$_4$: Ce powders. They have found that PL excitation spectra exhibit a broad band in the UV region, with a peak at 280 nm, and the emission spectrum shows a broad band in the visible region, with a peak in the blue region (400–650 nm) [3]. It seems that this kind of photoluminescence may be assigned to excitonic luminescence.

6. Light Yield Investigations

^{137}Cs pulse height spectra recorded with all the investigated crystals are presented in Figure 10.
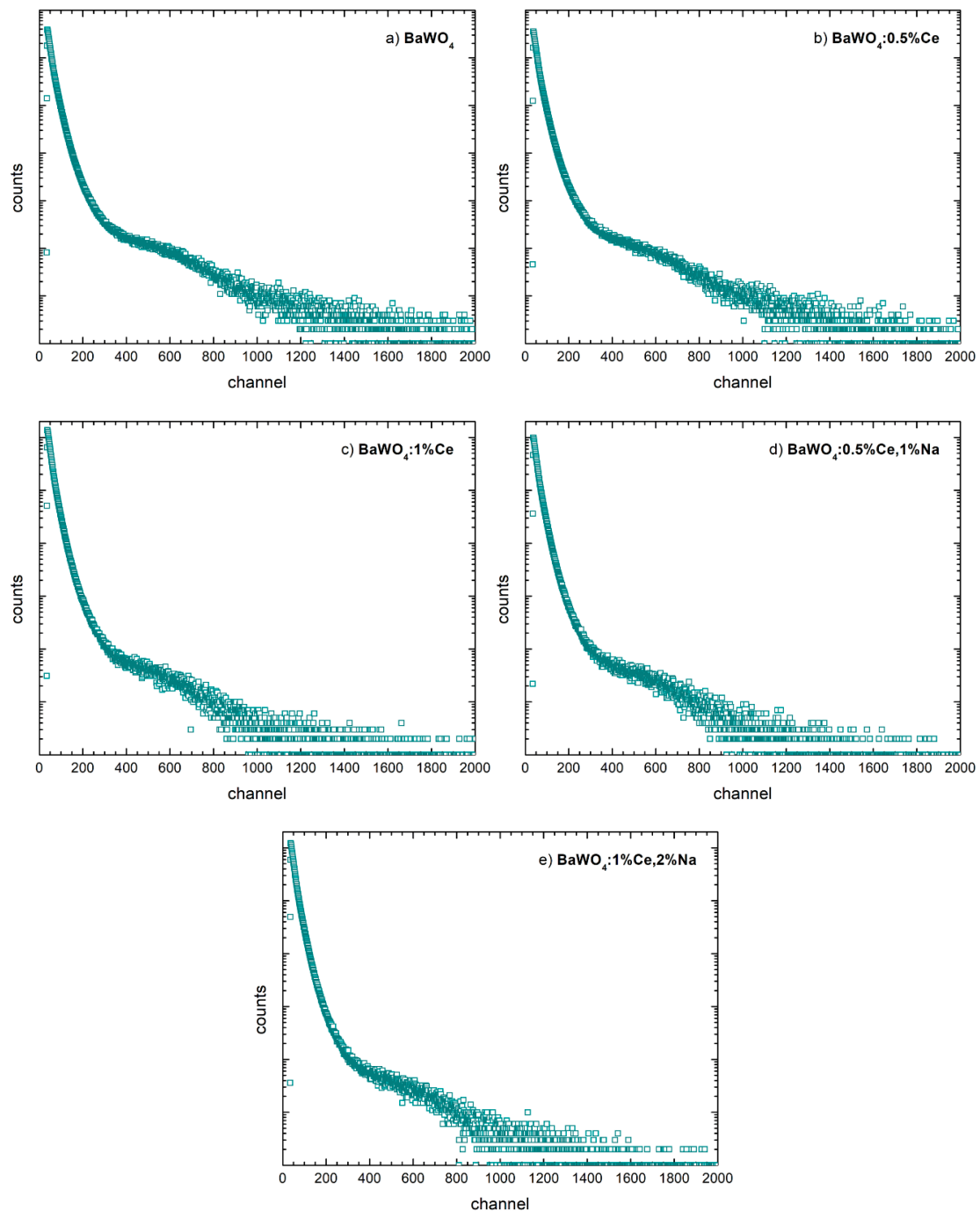

Figure 10. Pulse height spectra of the investigated samples: (**a**) BaWO$_4$; (**b**) BaWO$_4$: 0.5% Ce; (**c**) BaWO$_4$: 1% Ce; (**d**) BaWO$_4$: 0.5% Ce, 1% Na; (**e**) BaWO$_4$: 1% Ce, 2% Na.

They are all very similar, indicating that there is no influence of doping the crystals with Ce or co-doping with Na. None of the samples excited by gamma rays exhibit a clear full-energy peak (often referred to as a photo-peak), and only the Compton edge can be noticed somewhere close to channel 600. Considering the high gain (0.9×30) and long shaping time ($12 \mu s$), we get a clear indication that $BaWO_4$, either pure or doped/co-doped, is not a candidate for an efficient scintillation material. This conclusion agrees well with the results of radioluminescence studies.

7. Discussion and Conclusions

The good quality of the $BaWO_4$:Ce^{3+} 0.5 at. %; $BaWO_4$:Ce^{3+} 0.5 at. %, Na^+ 1 at. %; $BaWO_4$:Ce^{3+} 1 at. %; and $BaWO_4$: Ce^{3+} 1 at. %, Na^+ 2 at. % single crystals were obtained by the Czochralski grown method. The structure of the crystals is tetragonal and belongs to the $I4_1/a$ space group. The EPR angular dependencies allowed us to determine the SH parameters (in the crystallographic axis system) and to determine the symmetry of the substituted cerium ions. EPR measurements have shown that one isolated Ce^{3+} center of high C_4 symmetry could be found in the $BaWO_4$ single crystal and two or more others of lower symmetry, C_2, could be identified, depending on crystal doping and co-doping. In addition, in $BaWO_4$: Ce single crystals co-doped with sodium ions, we have observed EPR lines originating from cerium ions at the C_{2v} symmetry site. The introduction of sodium ions causes the crystal lattice to be better ordered by increasing the number of cerium ions in C_4 symmetry. Photoluminescence spectrum from the Ce^{3+} ions was not found. Only excitonic and defect centers luminescence in a range of 280 nm and 400–600 nm, respectively, have been detected. In a paper by Wlodarczyk et al. [19], optical spectroscopy of the above crystals has been analyzed under different values of external pressure. The authors of reference 19 have concluded that the observed luminescence has an excitonic character, independent of applied pressure. This is related to the location of Ce^{3+} 5d levels in the conduction band of the material. The luminescence is strongly temperature quenched, with a relatively small activation energy of a few meV [19]. Although Ce^{3+} does not show any emission centers, it contributes to the efficiency of exciton formation. It was observed in [19] that in crystals doped with Ce^{3+}, the exciton emission intensity is higher than in pure crystals.

References

1. Cerný, P.; Jelínková, H.; Basiev, T.T.; Zverev, P.G. Highly efficient picosecond Raman generators based on the $BaWO_4$ crystal in the near infrared, visible, and ultraviolet. *IEEE J. Quantum Electron.* **2002**, *38*, 1471–1478. [CrossRef]
2. Lacomba-Perales, R.; Ruiz-Fuertes, J.; Errandonea, D.; Martinez-Garcia, D.; Segura, A. Optical absorption of divalent metal tungstates: Correlation between the band-gap energy and the cation ionic radius. *EPL* **2008**, *83*, 37002. [CrossRef]
3. Dabre, K.V.; Dhoble, S.J.; Lochab, J. Synthesis and luminescence properties of Ce^{3+} doped MWO_4 (M = Ca, Sr and Ba) microcrystalline phosphors. *J. Lumin.* **2014**, *149*, 348–352. [CrossRef]
4. Oliveira, M.C.; Garcia, L.; Nogueira, I.C.; Gurgel, M.F.d.C.; Mercury, J.M.R.; Longo, E.; Andres, J. Synthesis and morphological transformation of $BaWO_4$ crystals: Experimental and theoretical insights. *Cer. Int.* **2016**, *42*, 10913–10921. [CrossRef]
5. Liu, L.; Zhang, S.; Bowden, M.E.; Chaudhuri, J.; de Yoreo, J.J. In Situ TEM and AFM Investigation of Morphological Controls during the Growth of Single Crystal $BaWO_4$. *Cryst. Growth Des.* **2018**, *18*, 1367–1375. [CrossRef]

6. Oliveira, M.C.; Andrés, J.; Gracia, L.; de Oliveira, M.S.M.P.; Mercury, J.M.R.; Longo, E.; Nogueira, I.C. Geometry, electronic structure, morphology, and photoluminescence emissions of $BaW_{1-x}Mo_xO_4$ (x = 0, 0.25, 0.50, 0.75, and 1) solid solutions: Theory and experiment in concert. *Appl. Surf. Sci.* **2019**, *463*, 907–917. [CrossRef]

7. Ke, J.; Younis, M.A.; Kong, Y.; Zhou, H.; Liu, J.; Lei, L.; Hou, Y. Nanostructured Ternary Metal Tungstate-based Photocatalysts for Environmental Purification and Solar Water Splitting: A Review. *Nan-Micro Lett.* **2018**, *10*, 69. [CrossRef] [PubMed]

8. Shi, Y.; Shi, J.; Dong, C. Luminescence characteristics and J-O analysis of $BaWO_4$: 3% Sm^{3+} crystal for yellow phosphors. *Cer. Int.* **2017**, *43*, 16356–16361. [CrossRef]

9. Brice, J.C.; Whiffin, P.A.C. Solute striate in pulled crystals of zinc tungstate. *Br. J. Appl. Phys.* **1967**, *18*, 581–691. [CrossRef]

10. Yang, F.G.; Tu, C.Y.; Wang, H.Y.; Wei, Y.P.; You, Z.Y.; Jia, G.H.; Li, J.F.; Zhu, Z.J.; Lu, X.A.; Wang, Y. Growth and spectroscopy of $ZnWO4$: Ho^{3+} crystal. *J. Alloy. Compd.* **2008**, *455*, 269–273. [CrossRef]

11. Errandonea, D.; Tu, C.Y.; Ha, G.H.; Martin, I.R.; Rodriguez-Mendoza, U.R.; Lahoz, F.; Torres, M.E.; Lavin, V. Effect of pressure on the luminescence properties of Nd^{3+} doped $SrWO_4$ laser crystal. *J. Alloy. Compd.* **2008**, *451*, 212–214.

12. Wlodarczyk, D.; Berkowski, M.; Głowacki, M.; Kaczmarek, S.M.; Kowalski, Z.; Brik, M.; Wittlin, A.; Przybylinska, H.; Zhydachevskii, Y.; Suchocki, A. Studies of Luminescence Efficiency of $BaWO_4$: Ce Crystals. In Proceedings of the 5th International Conference on Oxide Materials for Electronic Engineering—Fabrication, Properties and Application (OMEE-2017), Lviv, Ukraine, 29 May–2 June 2017. 232nd ECS Meeting, National Harbor, MD, USA, 1–5 October 2017.

13. Voronina, I.S.; Ivleva, L.I.; Basiev, T.T.; Zverev, P.G.; Polozkov, N.M. Active Roman media: $SrWO_4$:Nd^{3+}, $BaWO_4$:Nd^{3+}, growth and characterization. *J. Optoelectron. Adv. Mater.* **2003**, *5*, 887–892.

14. Sleight, A.W. Accurate cell dimensions for ABO4 molybdates and tungstates. *Acta Crystallogr. B* **1972**, *28*, 2899–2902. [CrossRef]

15. Mombourquette, M.J.; Weil, J.A.; McGavin, D.G. *EPR–NMR User's Manual*; Department of Chemistry, University of Saskatchewan: Saskatoon, SK, Canada, 1999.

16. Zhang, H.; Liu, T.; Zhang, Q.; Wang, X.; Yin, J.; Song, M.; Guo, X. First-principles study on electronic structures of $BaWO_4$ crystals containing F-type color centers. *J. Phys. Chem. Solids* **2008**, *69*, 1815–1819. [CrossRef]

17. Leniec, G.; Kaczmarek, S.M.; Bodziony, T.; Fuks, H.; Kowalski, Z.; Berkowski, M.; Głowacki, M. Site symmetries of cerium ions in $BaWO_4$ single crystals codoped with sodium ions. *Appl. Magn. Res.* **2019**. [CrossRef]

18. Cavalcante, L.S.; Sczancoski, J.C.; Lima, L.F., Jr.; Espinosa, J.W.M.; Pizani, P.S.; Varela, J.A.; Longo, E. Synthesis, Characterization, Anisotropic Growth and Photoluminescence of $BaWO_4$. *Cryst. Growth Des.* **2009**, *9*, 1002–1012. [CrossRef]

19. Wlodarczyk, D.; Bulyk, L.-I.; Berkowski, M.; Glowacki, M.; Kaczmarek, S.M.; Kowalski, Z.; Wittlin, A.; Przybylinska, H.; Zhydachevskii, Y.; Suchocki, A. High Pressure and low-temperature optical studies of $BaWO_4$: Ce, Na. *J. Mater. Chem. C* **2019**. under review.